



Research article

Improved super-twisting sliding mode control strategy in permanent magnet synchronous motors for hydrogen fuel cell centrifugal compressor

Li Dong^a, Pei Jiang^{b,*}^a College of Weapon Engineering, Naval University of Engineering, Wuhan, 430033, China^b Wuhan Institute of Shipbuilding Technology, Wuhan, 430050, China

ARTICLE INFO

Keywords:

Sliding mode control
Permanent magnet synchronous motor
Hydrogen fuel cell
Super-twisting algorithm

ABSTRACT

This paper rigorously addresses the intricate control demands of high-speed, high-pressure, wide adjustable speed range, and high energy utilization efficiency required in hydrogen fuel cell centrifugal compressor, with a focus on the speed control of 40,000 RPM permanent magnet synchronous motors (PMSMs). An improved second-order super twisting sliding mode control (STSMC) strategy is proposed to enhance system stability and robustness by integrating the beetle antennae search (BAS) algorithm and grey wolf optimization (GWO) algorithm. The global search capability of BAS is used to improve the local optima issues of GWO, and then the improved GWO algorithm is utilized to address the issues related to parameter selection and convergence speed inherent in the STSMC. Theoretical validity of the proposed strategy is asserted through Quadratic Lyapunov Function, and its practicality is affirmed by thorough simulation. Comparative analyses are conducted with PI controller, traditional Sliding Mode Controller (SMC), and standard Super-Twisting Sliding Mode Controller (ST) under several case studies to show the superiority of the propose STSMC.

1. Introduction

In response to escalating global energy crises and environmental degradation, there is an increasing shift toward Electric Vehicles (EVs). Prominent automotive producers from countries such as Germany, the UK, and France have announced intentions to halt the production of internal combustion engine vehicles. Notably, China's 'Electric Vehicle Industry Development Plan (2021–2035)' aims for EVs to constitute a 40 % share of total vehicle sales by 2030 [1,2]. EVs that do not rely on fossil fuels and have zero emissions can ease the pressure of fossil fuel scarcity and environmental pollution. However, battery technology in EVs faces formidable challenges in extending vehicle range and safety concerns due to battery combustion [3], underscore the pressing need for research in hydrogen fuel cell technology. Such technology not only offers the prospect of extended driving ranges and a marked reduction in battery fire risks but also holds considerable future market potential. This highlights the strategic and practical significance of investigating hydrogen fuel cells for the further advancement and popularization of EV technology.

The hydrogen fuel cell power system is comprised of four subsystems: the fuel cell stack, the cathode air supply system, the anode hydrogen supply system, and the water-heat management system [4,5]. The core of the cathode air supply subsystem is a centrifugal

* Corresponding author.

E-mail address: peij_wit@hotmail.com (P. Jiang).

<https://doi.org/10.1016/j.heliyon.2024.e24181>

Received 17 August 2023; Received in revised form 24 December 2023; Accepted 4 January 2024

Available online 5 January 2024

2405-8440/© 2024 The Authors. Published by Elsevier Ltd. This is an open access article under the CC BY-NC-ND license (<http://creativecommons.org/licenses/by-nc-nd/4.0/>).

compressor driven by a high-speed motor. This compressor is designed to pressurize the air and regulate the appropriate air mass flow rate, subsequently enhancing the fuel cell's power density and operating efficiency. Such operations directly influence the overall system efficiency and cost. Critical requirements for centrifugal compressor encompass high speed and high pressure to satisfy the oxygen supply and system power demands, and a broad speed range to address varying operational demands and swiftly adapt to load changes. Furthermore, high energy utilization efficiency is sought to minimize energy wastage during air compression, enhance the system's overall energy efficiency, and subsequently reduce both operational expenses and environmental ramifications. To fulfill these outlined requirements for the centrifugal compressor, its drive motor must maintain a substantial speed and power.

Permanent Magnet Synchronous Motors (PMSM) are characterized by superior power density, unit volume and mass output torque, starting torque, peak rotational speed, braking performance, and reduced torque ripple [6,7]. These advantages are consistent with the requirements of the drive motor in fuel cell centrifugal compressors, which encompass rapid response, compact size, substantial torque, and a broad range of speed control. The rotational speed of the drive motor for a hydrogen fuel cell centrifugal compressor is contingent on the specific compressor design and application needs, typically oscillating between 15,000 and 50,000 rpm. However, these speeds can induce noise, vibration, and mechanical wear issues, making discerning design and control. Given the complex operating conditions of fuel cells and their vulnerability to various adverse factors, emphasis must be placed on deploying robust and stable speed controller algorithms to ensure system reliability and stability.

Advanced control theories and algorithms, including intelligent control, sliding mode control, model predictive control, adaptive control, and robust control, have been progressively integrated to PMSM, addressing the limitations of PID controllers in multivariable, nonlinear, and strongly coupled systems [8–10]. Sliding mode control, recognized for its robustness, rapid response, and straightforward implementation without online identification, has been widely adopted. However, it also possesses inherent limitations, such as slow convergence, uncertain upper boundary of disturbance, and noticeable chattering. Various advanced methods have been employed to mitigate these challenges, incorporating exponential approach law [11], power reaching law [12], and variable-rate reaching law [13], as well as the introduction of quasi-sliding modes and boundary layer concepts to suppress chattering [14,15]. Traditional sliding mode control, adopting a linear sliding surface, achieves system error convergence gradually. However, it is challenged by the inability of differential and integral sliding mode controls to converge system error within a finite time [16,17]. To address the slow convergence and chattering, second-order sliding mode control method was innovated to enable accurate robust differentiation and sustaining system states at zero [18]. Despite the improvements, practical application remains stymied by discontinuities in the control function and complex responses. Intelligent control approaches such as fuzzy control, neural networks, and genetic algorithms, have been incorporated to further reduce system chattering. Among these, super-twisting algorithm, a second-order sliding mode control algorithm, offers the distinct advantage of obviating the need to calculate the derivatives or differences of the sliding variables [19]. But it also exhibits several drawbacks: a reliance on disturbance boundary information for parameter selection, slower convergence rates near equilibrium points, an inability to converge with smaller neighborhoods due to fixed power in nonlinear terms, and increased complexity in stability analysis upon incorporating linear terms [20]. To overcome these limitations, an improved global second-order super twisting sliding mode control (STSMC) strategy is proposed in this paper, which effectively amalgamates the strengths of beetle antennae search (BAS) and grey wolf optimization (GWO) algorithms.

Comparing with the existing sliding mode control approaches, the key contributions of this work include:

- 1) An improved second-order super-twisting sliding mode control strategy is proposed to improve the disturbance rejection ability and dynamic performance of PMSM to meet practical application requirements for fuel cell centrifugal compressors.
- 2) The proposed strategy integrates BAS into GWO, enhancing global search capabilities and addressing shortcomings in parameter selection of the traditional super-twisting algorithm.
- 3) Detailed stability analyses of the proposed STSMC strategy are provided to certify its finite-time convergence.

In the following, Section 2 introduces the mathematical model of PMSM and its vector control system. In Section 3, the advantages of BAS and GWO are combined to optimize the control parameters in STSMC, and the finite-time convergence of the proposed strategy are analytically evaluated. Section 4 validates the viability and effectiveness of STSMC through comparative simulations with conventional sliding mode controller, super twisting sliding mode controller, and PI controller. Section 5 provides the conclusion.

2. PMSM and sliding mode control

2.1. Mathematical model of PMSM in rotating coordinate system

The proposed control strategy for PMSM is constructed in synchronous rotating coordinate system. Assuming the PMSM has negligible cross-coupling magnetic saturation, structural asymmetry, and iron losses, and disregarding magnet eddy current loss and harmonics in the characterization functions of windings, rotor anisotropy, and the coercive force of magnets, the stator voltages are shown in Equation (1).

$$\begin{bmatrix} u_d \\ u_q \end{bmatrix} = \begin{bmatrix} R_s & 0 \\ 0 & R_s \end{bmatrix} \begin{bmatrix} i_d \\ i_q \end{bmatrix} + \frac{d}{dt} \begin{bmatrix} \psi_d \\ \psi_q \end{bmatrix} + \begin{bmatrix} -\omega_e \psi_q \\ \omega_e \psi_d \end{bmatrix} \quad (1)$$

where u_d and u_q are the equivalent voltage vectors in the rotating coordinate system, i_d and i_q are the current vectors, ψ_d and ψ_q are the rotor flux, R_s is the stator resistance. ω_e is the rotor angular velocity.

The stator flux is shown in Equation (2).

$$\begin{bmatrix} \psi_d \\ \psi_q \end{bmatrix} = \begin{bmatrix} L_d & 0 \\ 0 & L_q \end{bmatrix} \begin{bmatrix} i_d \\ i_q \end{bmatrix} + \psi_f \begin{bmatrix} 1 \\ 0 \end{bmatrix} \quad (2)$$

where L_d and L_q are the rotor inductance. ψ_f is the permanent magnet flux linkage.

The electromagnetic torque is given by Equation (3).

$$T_e = \frac{3}{2} p_n i_q [i_d (L_d - L_q) + \psi_f] \quad (3)$$

where T_e is the electromagnetic torque, and p_n is the number of rotor pole pairs.

The motion is shown in Equation (4).

$$T_e - T_l - B\omega_m = J \frac{d\omega_m}{dt} \quad (4)$$

where T_l is the load torque, J is the rotor inertia, B is the viscous friction coefficient, and ω_m is the mechanical angular velocity, $\omega_e = p_n \omega_m$.

2.2. PMSM sliding mode control

This paper proposes an advanced sliding mode controller as an improvement to the conventional vector control approach widely applied in PMSM. Traditionally, such vector control systems comprise a speed controller that regulates speed signals to obtain the current i_q^* , a current controller to sustain steady current vectors, and a Pulse Width Modulation (PWM) module responsible for calculating the duty cycle to govern the output voltage and current. In order to achieve optimal torque output, the $i_d = 0$ strategy is employed here. Under this strategy, by setting i_d to zero, the contribution of the motor's d-axis to the torque is negated. Consequently, all of the current in PMSM is utilized solely for the generation of electromagnetic torque. This approach simplifies the control process, as only i_q needs to be regulated to control the motor's torque. The output current and voltage from the three-phase inverter are collected, allowing the reconstruction of the dq -axis current essential for current feedback. Concurrently, the rotor speed is collected for the speed control loop.

The PMSM speed control block diagram based on the proposed STSMC is shown in Fig. 1. Differing from conventional vector control, this paper replaces the speed PID controller with a second-order super-twisting sliding mode controller to generate the reference value of the q-axis current.

Equation (4) demonstrates the equation of motion for PMSM, which can be rewritten as Equation (5).

$$J\dot{\theta} = T_e - B\dot{\theta} - T_l = k_t u - B\dot{\theta} - T_l \quad (5)$$

where θ is the rotor angle, $\dot{\theta} = \omega$. u is the reference value of the q-axis current, $k_t = \frac{3}{2} p_n \psi_f$.

The traditional sliding mode function is given by Equation (6).

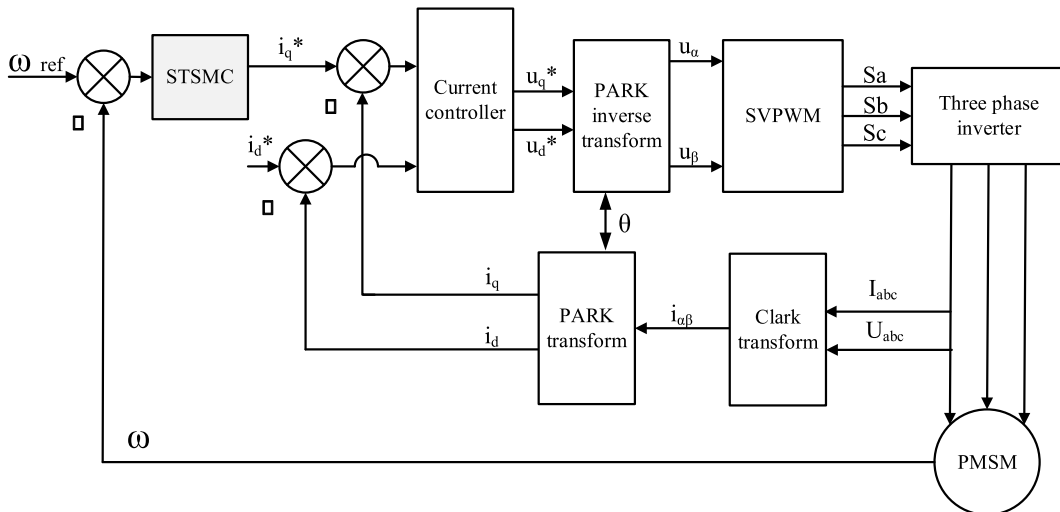


Fig. 1. Control block diagram of PMSM based on STSMC.

$$s(t) = ce(t) + \dot{e}(t) \quad (6)$$

where $e(t)$ is the error, and $c > 0$.

Let $e = \theta_{ref} - \theta$, and $\dot{e} = \omega_{ref} - \omega$, using Equation (5) and Equation (6), we can get Equation (7).

$$\dot{s} = c\dot{e} + \ddot{e} = c\dot{e} + \ddot{\theta} - \frac{1}{J}(k_t u - B\dot{\theta} - T_l) \quad (7)$$

where θ_{ref} is the reference rotor angle, and ω_{ref} is the reference rotor speed.

To ensure the system stability, the Lyapunov function is defined as Equation (8).

$$V(t) = \frac{1}{2}s^2 \quad (8)$$

Using Equation (7), the derivative of Equation (8) yields:

$$\dot{V} = s\dot{s} = s\left(c\dot{e} + \ddot{\theta} - \frac{1}{J}(k_t u - B\dot{\theta} - T_l)\right) \quad (9)$$

To make the derivative of the Lyapunov function negative definite, it is required that $\dot{s} \leq 0$. Let:

$$\dot{s} = c\dot{e} + \ddot{\theta} - \frac{1}{J}(k_t u - B\dot{\theta} - T_l) = -\varepsilon \text{sgn}(s) \quad (10)$$

where $\text{sgn}(\cdot)$ is the sign function and ε is the upper boundary of the disturbance, from Equation (10), we have:

$$u = \frac{J}{k_t} \left(c\dot{e} + \varepsilon \text{sgn}(s) + \ddot{\theta} + \frac{B}{J}\dot{\theta} + \frac{1}{J}T_l \right) \quad (11)$$

In practical engineering applications, the load torque T_l is an uncontrollable and uncertain factor which should not be treated as a manipulable input. Consequently, using Equations (9) and (11), the derivative of the Lyapunov function will be transformed as:

$$\begin{aligned} \dot{V} &= s \left(c\dot{e} + \ddot{\theta} - \frac{1}{J} \left(Jc\dot{e} + J\varepsilon \text{sgn}(s) + J\ddot{\theta} + B\dot{\theta} - B\dot{\theta} - T_l \right) \right) \\ &= s \left(-\varepsilon \text{sgn}(s) + \frac{1}{J}T_l \right) = -\varepsilon|s| + \frac{1}{J}sT_l \end{aligned} \quad (12)$$

Equation (12) suggests that when $\varepsilon \geq T_l/J$, $\dot{V} \leq 0$. To ensure system robustness, it is necessary to increase the upper limit of the disturbance ε to prevent excessive disturbances from destabilizing the system. However, an excessively large ε could exacerbate chattering, thereby causing adverse effects. Therefore, current research primarily aims to reduce the occurrence of chattering while ensuring system robustness.

3. Improved STSMC incorporating BAS and GWO

3.1. Improved STSMC

The improved STSMC is proposed by analyzing the characteristics of the PMSM speed control system and integrating GWO and BAS to optimize the parameters of the super-twisting algorithm. This strategy can adjust speed based on the distance from the sliding mode surface and enhance the system response speed.

The traditional super-twisting algorithm is formulated as Equation (13).

$$\begin{cases} \dot{x}_1 = -l_1|x_1|^{\frac{1}{2}}\text{sign}(x_1) + x_2\dot{x}_2 = -l_2\text{sign}(x_1) \end{cases} \quad (13)$$

where x_1 and x_2 are state variables, $l_1 > 0$, $l_2 > 0$.

Using the rapid terminal sliding mode surface:

$$s = \dot{x} + \alpha x + \beta \dot{x}^{\frac{q}{p}} \quad (14)$$

where $x = e$, $\alpha > 0$, $\beta > 0$, p and q are positive odd, $p > q$.

The differential of Equation (14) can be expressed by:

$$\dot{s} = \ddot{e} + \alpha\dot{e} + \beta\frac{q}{p}\dot{e}^{\frac{q}{p}-1}\dot{\dot{e}} = \ddot{\omega}_{ref} - \frac{1}{J}(k_t u - B\dot{\omega} - T_l) + \alpha\dot{e} + \beta\frac{q}{p}\dot{e}^{\frac{q}{p}-1}\dot{\dot{e}} \quad (15)$$

Employing Equation (13) as the approach law, so the convergence of the sliding mode surface and its derivative can be ensured to

zero:

$$\dot{s} = -l_1 |s|^{\frac{1}{2}} \text{sign}(s) + \int (-l_2 \text{sign}(s)) \quad (16)$$

Combining Equation (15) with Equation (16), the following control law is derived as Equation (17).

$$u^* = \frac{J}{k_t} \left(\dot{\omega}_{ref} + \frac{B}{J} \omega + a \dot{e} + \frac{\beta q}{p} e^{p-1} \dot{e} + l_1 |s|^{\frac{1}{2}} \text{sign}(s) + l_2 \int \text{sign}(s) \right) \quad (17)$$

where T_l is an uncertain factor which should not be included in the control law.

3.2. Integration of BAS into GWO for enhanced global search

In the proposed STSMC strategy, there are numerous parameters in the sliding mode portion. A considerable amount of time is required to tune these parameters to achieve satisfactory control performance. To enhance efficiency and also improve parameter accuracy, optimization algorithms are subsequently employed for parameter tuning.

This study introduces a novel global search algorithm that assimilates the strengths of GWO and BAS to overcome specific limitations, particularly the susceptibility of the former to getting trapped in local optima. The conventional GWO can see a substantial increase in time and spatial complexity when employed in larger operational scenarios. By incorporating BAS, the proposed algorithm enables the performance of both local and global searches while circumventing local optima.

Since BAS is a single-unit search algorithm, its incorporation into GWO empowers the initial wolf individuals to maximize the utilization of solution space information, consequently improve the global search capability. In addition to this, this novel algorithm is further integrated with the Super-Twisting algorithm, providing optimized parameter selections to suppress its inherent chattering issue.

The proposed algorithm primarily maintains the integrity of the GWO while dividing each two-wolf pair into a group and initializing them according to the two antennae of a beetle. Initially, the wolves are ranked according to the fitness level. The top three groups of wolves, with superior fitness, are denoted as α , β , and δ , while the remaining wolves are denoted as ω . Lower-ranking wolf groups must follow the commands of the higher-ranking groups. The optimization process is conducted under the direction of the dominant wolf groups, leading the wolves to track, encircle, and attack the target. The mathematical model for encircling the target is described as Equation 18–21.

$$D = C \circ X_p(t) - X(t) \quad (18)$$

$$X(t+1) = X_p(t) - A \circ D \quad (19)$$

$$A = 2a \circ r_1 - a \quad (20)$$

$$C = 2r_2 \quad (21)$$

where t is the current iteration, \circ is the basic product operation, D is the distance between wolf and target, $X_p(t)$ is the position vector of target, $X(t)$ is the current position of wolves, A and C are collaborative coefficient vectors, a will gradually decrease throughout the iteration process, declining linearly from 2 to 0, r_1 and r_2 are random vectors within the interval [0,1].

The position of wolf group α in each iteration is shown in Equation (22).

$$\begin{cases} X_{\alpha 1} = X_t + l * \vec{d} \\ X_{\alpha 2} = X_t - l * \vec{d} \end{cases} \quad (22)$$

where l represents the distance between the centroid of beetle and its antennae, \vec{d} is a random unit vector.

After the same normalization process as BAS, combining Equation (19) and Equation (22), the position of wolf group α is determined based on the difference in the scent intensity perceived by the two antennae:

$$X_\alpha = X_t + \delta_t * \vec{d} * \text{sign}[f(X_{\alpha 1}) - f(X_{\alpha 2})] \quad (23)$$

where δ_t is the exploration step size, $f(\cdot)$ is the fitness function, which can be defined as Equation (24).

$$f = \frac{1}{N} \sum_{n=1}^N [|\omega_{ref}(n) - \omega(n)| n T_s] \quad (24)$$

where T_s is the sampling time, N is the number of sampling points.

Similar to Equation (23), the position of wolf group β , δ , and ω are shown in Equation 25–27.

$$X_\beta = X_t + \delta_t * \vec{d} * \text{sign}[f(X_{\beta 1}) - f(X_{\beta 2})] \quad (25)$$

$$X_\delta = X_t + \delta_t * \vec{d} * \text{sign}[f(X_{\delta 1}) - f(X_{\delta 2})] \tag{26}$$

$$X_{\omega} = X_t + \delta_t * \vec{d} * \text{sign}[f(X_{\omega 1}) - f(X_{\omega 2})] \tag{27}$$

After each iteration, the better α , β , and δ are determined based on the position of each wolf, until the optimal solution is finally found. The formula for the positions of α , β , and δ after each iteration can be derived as Equation28–30.

$$\vec{X}_1 = \vec{X}_\alpha - A_1 \cdot \vec{D}_\alpha \tag{28}$$

$$\vec{X}_2 = \vec{X}_\beta - A_2 \cdot \vec{D}_\beta \tag{29}$$

$$\vec{X}_3 = \vec{X}_\delta - A_3 \cdot \vec{D}_\delta \tag{30}$$

where \vec{X}_α , \vec{X}_β , and \vec{X}_δ are the positions of the optimal three groups of grey wolves in current population, from Equation (18), \vec{D}_α , \vec{D}_β , and \vec{D}_δ are the distance between the optimal three wolf groups and the subsequent wolf position vectors, which can be derived as Equation 31–33.

$$\vec{D}_\alpha = \left| \vec{C}_1 \cdot \vec{X}_\alpha - \vec{X}_t \right| \tag{31}$$

$$\vec{D}_\beta = \left| \vec{C}_2 \cdot \vec{X}_\beta - \vec{X}_t \right| \tag{32}$$

$$\vec{D}_\delta = \left| \vec{C}_1 \cdot \vec{X}_\delta - \vec{X}_t \right| \tag{33}$$

The position of current candidate wolf is shown in Equation (34).

$$\vec{X}(t+1) = \frac{\vec{X}_1 + \vec{X}_2 + \vec{X}_3}{3} \tag{34}$$

When the absolute value of A is greater than 1, the wolves disperse in different regions to search for target. Otherwise, the wolves will congregate in certain areas for focused hunting. The hunt continues until the optimal location is found, after which an attack is initiated.

As the number of iterations increases, the search step size needs to be modified adaptively decreasing, which can be defined as Equation (35).

$$\delta_t = k\delta_{t-1} \tag{35}$$

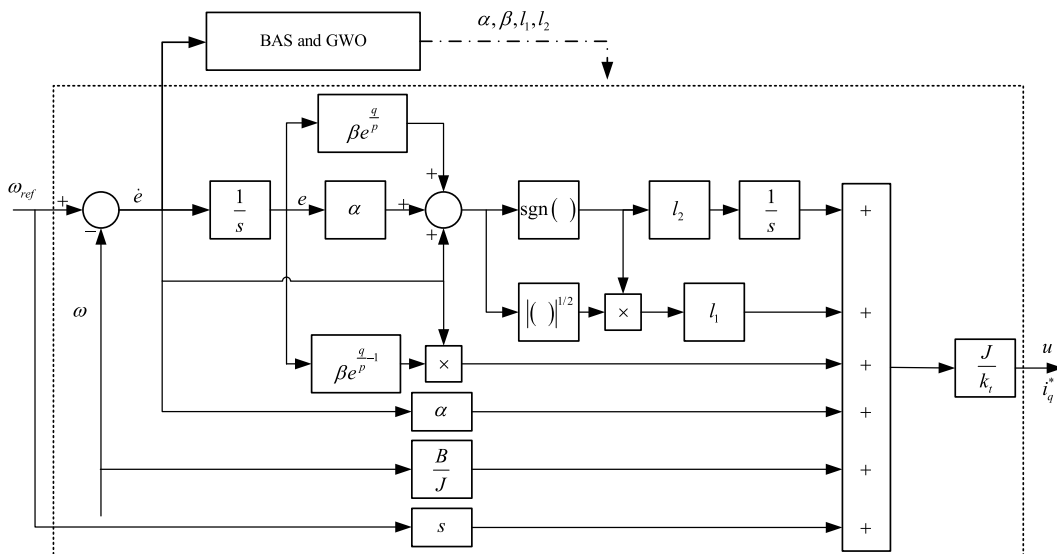


Fig. 2. Block diagram of PMSM speed controller based on improved STSMC.

where k is the step decay coefficient.

Combining the PMSM control based on the improved STSMC, the speed control block for PMSM is illustrated in Fig. 2. BAS and GWO selects the optimal parameter combination in each iteration and continues iterating until the maximum number of iterations is reached. The steps of applying these algorithms are as follows:

Step 1. Generate parameters α, β, l_1, l_2 randomly.

Step 2. Substitute the parameters into Simulink model, run simulation and collect data necessary for calculating the fitness function.

Step 3. Select the best parameters with smallest $f(\cdot)$, and move to the next iteration.

3.3. Stability analysis of improved STSMC

To prove that the improved STSMC is robust and globally stable, the first step is to prove the finite-time convergence. Define the quadratic Lyapunov function as Equation (36).

$$V = \zeta^T P \zeta \tag{36}$$

where P is the positive definite symmetric matrix satisfying the Lyapunov equation $A^T P + PA = -Q$, and $A = \begin{bmatrix} -l_1 & 1 \\ -l_2 & 0 \end{bmatrix}$, Q is an arbitrary positive definite symmetric matrix. Since $l_1, l_2 > 0$, then A is Hurwitz matrix. $\zeta^T = [|s|^{\frac{1}{2}} \text{sign}(s), -\int l_2 \text{sign}(s)]$.

The derivative of ζ is shown in Equation (37).

$$\dot{\zeta} = \begin{bmatrix} \varphi(s)\dot{s} \\ -l_2 \text{sign}(s) \end{bmatrix} = \varphi(s) \begin{bmatrix} -l_1 |s|^{\frac{1}{2}} \text{sign}(s) - \int (l_2 \text{sign}(s)) \\ -l_2 |s|^{\frac{1}{2}} \text{sign}(s) \end{bmatrix} = \varphi(s) \begin{bmatrix} -l_1 & 1 \\ -l_2 & 0 \end{bmatrix} \begin{bmatrix} |s|^{\frac{1}{2}} \text{sign}(s) \\ \int (-l_2 \text{sign}(s)) \end{bmatrix} \tag{37}$$

Define $\varphi(s) = k_1 + k_2 |s|^{-\frac{1}{2}}, k_{1,2} > 0$. From Equations (36) and (37), we can get:

$$\dot{V} = \dot{\zeta}^T P \zeta + \zeta^T P \dot{\zeta} = \varphi(s) \zeta^T (A^T P + PA) \zeta = -\varphi(s) \zeta^T Q \zeta \tag{38}$$

It can be concluded that \dot{V} is negative definite, indicating the system exhibits asymptotic stability over a wide range. Considering that $V = \zeta^T P \zeta$ is a quadratic positive-definite function, we can obtain Equation (39).

$$\lambda_{\min}\{P\} \|\zeta\|_2^2 \leq V \leq \lambda_{\max}\{P\} \|\zeta\|_2^2 \tag{39}$$

where $\|\zeta\|_2$ is the second order paradigm on Euclidean space, $\lambda_{\max}\{P\}$ and $\lambda_{\min}\{P\}$ are the maximum and minimum eigenroot of P , respectively.

$$\|\zeta\|_2^2 = |s| + \left(\int (-l_2 \text{sign}(s)) \right)^2, |s|^{\frac{1}{2}} \leq \|\zeta\|_2 \leq \frac{V^{\frac{1}{2}}}{\lambda_{\min}^{\frac{1}{2}}\{P\}} \tag{40}$$

Combining Equation 38–40, we can get:

$$\begin{aligned} \dot{V} &= -\varphi(s) \zeta^T Q \zeta \leq -\varphi(s) \lambda_{\min}\{Q\} \|\zeta\|_2^2 = -k_1 \lambda_{\min}\{Q\} \|\zeta\|_2^2 - k_2 |s|^{-\frac{1}{2}} \lambda_{\min}\{Q\} \|\zeta\|_2^2 \\ &\leq -k_1 \frac{\lambda_{\min}\{Q\}}{\lambda_{\max}\{P\}} V - k_2 |s|^{-\frac{1}{2}} \frac{\lambda_{\min}\{Q\}}{\lambda_{\max}\{P\}} V = -k_1 \frac{\lambda_{\min}\{Q\}}{\lambda_{\max}\{P\}} V - k_2 \frac{\lambda_{\min}\{Q\} \lambda_{\min}^{\frac{1}{2}}\{P\}}{\lambda_{\max}\{P\}} V^{\frac{1}{2}} \end{aligned} \tag{41}$$

Let $\gamma_1(Q, P, k_1) = k_1 \frac{\lambda_{\min}\{Q\}}{\lambda_{\max}\{P\}}, \gamma_2(Q, P, k_2) = k_2 \frac{\lambda_{\min}\{Q\} \lambda_{\min}^{\frac{1}{2}}\{P\}}{\lambda_{\max}\{P\}}$, and:

$$\dot{V} = -\gamma_1 V - \gamma_2 V^{\frac{1}{2}} \tag{42}$$

Change Equation (42) as:

$$\dot{y} + \frac{\gamma_1}{2} y = -\frac{\gamma_2}{2} \tag{43}$$

where $y = V^{\frac{1}{2}}, \dot{y} = \frac{1}{2} V^{-\frac{1}{2}} \dot{V}$, solve Equation (43), we can get:

$$y = -\frac{\gamma_2}{\gamma_1} + \frac{\gamma_2}{\gamma_1} e^{-\frac{\gamma_1}{2} t} + y(0) e^{-\frac{\gamma_1}{2} t} \tag{44}$$

Let $y = 0$, so the convergence time is as shown in Equation (45).

$$t_s = \frac{2}{\gamma_1} \ln \left(1 + \frac{\gamma_1}{\gamma_2} V^{\frac{1}{2}}(0) \right) \tag{45}$$

when $\gamma_1 = 0$ or $\gamma_2 = 0$, the Lyapunov function exhibits a simple exponential convergence. Then, we can derive:

Theorem 1. *Considering the sliding mode surface (14) and speed control law (17), the proposed STSMC secures global stability, guaranteeing system convergence to zero within a finite time.*

4. Experimental verification

Based on the speed controller designed in Fig. 2 and the theoretical foundation of PMSM, simulations were conducted in Matlab/Simulink considering disturbances on the load side. In the constructed simulation system, a control structure incorporating an external speed loop and an internal current loop was employed, utilizing $i_d = 0$ control strategy. Subsequently, modules including coordinate transformations (Clark and Park, along with their respective inverse transformations), SVPWM, PMSM motor models, and power supply were established. The final schematic of the PMSM simulation system is presented in Fig. 3, and the parameters of PMSM are shown in Table 1.

To validate the effectiveness of the proposed STSMC, four cases are conducted under various operating conditions of the PMSM. Comparative analyses were undertaken using three different control methods: PI controller, traditional Sliding Mode Controller (SMC), and standard Super-Twisting Sliding Mode Controller (ST) to substantiate the robustness of the proposed strategy. All the simulations are performed in MATLAB R2020a environment on a PC with i7-12700H CPU with 16 GB RAM.

4.1. Case 1: variable load condition

To address the load disturbances that occur during the operation of the PMSM, the first case was designed in which the motor starts at a no-load constant speed of 1000 r/min. The load is suddenly increased to 10 N • m at 0.2s and decreased to 10 N • m at 0.3s, and the simulation results are shown in Fig. 3. This procedure is conducted to validate the enhanced robustness exhibited by the proposed STSMC strategy.

From Fig. 4, it can be observed that the overshoot of the proposed STSMC is 5.553 r/min when the speed increases to 1000 r/min. At $t = 0.01s$, the motor speed stabilizes at the set value of 1000 r/min. After applying a fixed load torque of 10 N m, the speed of the proposed STSMC decreases to 982.823 r/min and returns to the set value at $t = 0.208s$. The detailed value of performance indexes are given in Table 2.

From Table 2, the overshoot of the proposed STSMC is 0.55 %, which is a 98.4 % reduction compared to PI controller and a 93.7 % reduction compared to ST. In terms of response speed, the settling time of STSMC is 0.01s, a 90 % improvement over PI controller, and 28.6 % faster than the ST. Regarding steady-state performance, STSMC has a steady-state error of 0.019r/min, a 91.2 % improvement over PI controller, and a 57.8 % improvement over ST. These results indicate that OSA-SMC can reach steady-state faster and with minimal oscillation during no-load startup, demonstrating its superior no-load startup performance compared to other comparative methods.

From Tables 3 and 4, it can be observed that, when the load torque suddenly increases, the overshoot of STSMC is 1.718 %, which is 76.4 % smaller than PI control and 0.8 % smaller than ST. When the load torque suddenly decreases, the overshoot of STSMC is 1.693

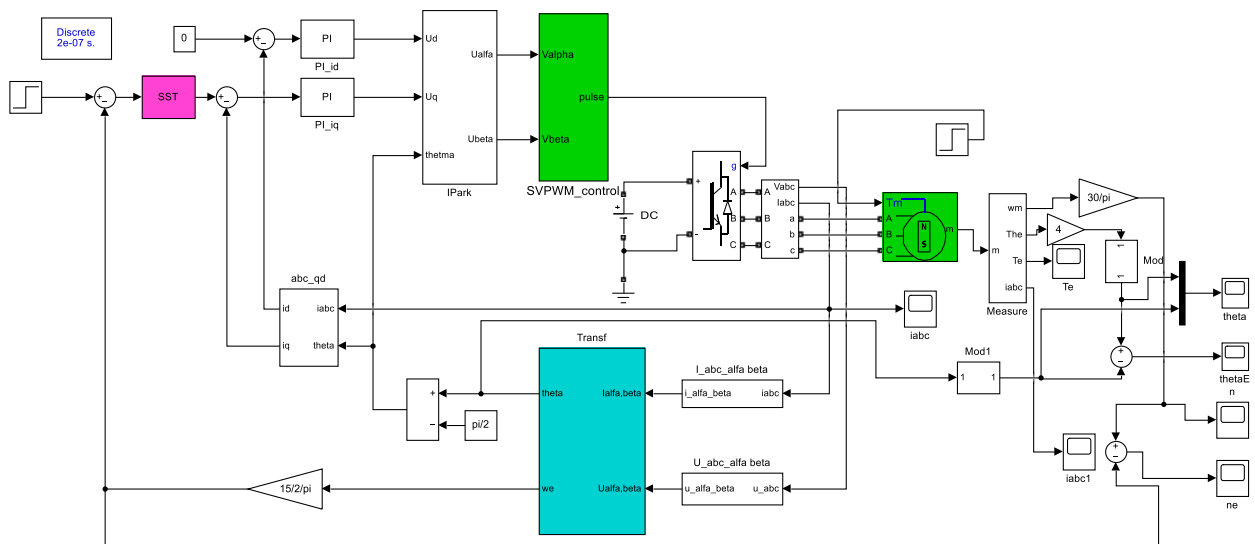


Fig. 3. PMSM model build in Matlab/Simulink.

Table 1
Parameters of PMSM.

Parameters	Value
Stator resistance R_s	2.356 Ω
d-axis inductance L_d	0.83 mH
q-axis inductance L_q	0.83 mH
Stator magnetic flux ψ_f	0.1225 Wb
Pole pairs	4
Rotational inertia J	0.003 $\text{kg} \cdot \text{m}^2$
DC bus voltage	311 V
Friction coefficient B	0.008 $\text{N} \cdot \text{m} \cdot \text{s}$

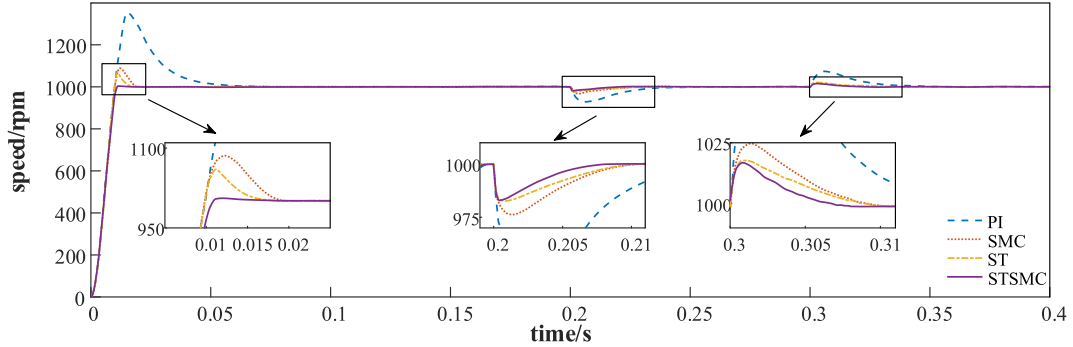


Fig. 4. Simulation results for case 1.

Table 2
Performance index during the start of case 1.

Control method	Peak RPM/ (r/min)	RPM overshoot/(%)	Settling time/(s)	Steady-state error/(r/min)	Torque overshoot/($\text{N} \cdot \text{m}$)
PI	1351.444	35.144	0.046	0.217	7.537
SMC	1088.391	8.839	0.017	0.05	6.042
ST	1061.236	6.124	0.014	0.045	5.547
STSMC	1005.553	0.555	0.01	0.019	0.574

%, which is 76.7 % smaller than PI control and 5.1 % smaller than ST. Regarding the response speed, the settling time of STSMC is 0.008s, which is 74.2 % faster than PI control and 33.3 % faster than ST. This indicates that when faced with sudden increases or decreases in load torque, STSMC has better robustness than PI control. When the load torque suddenly increases, there’s only a 0.8 % difference between STSMC and ST. When the load torque suddenly decreases, there’s only a 5.1 % difference between them. However, in terms of speed, STSMC is 33 % faster than ST, indicating that STSMC can return to a stable state more quickly.

4.2. Case 2: startup with load

To deal with the challenges associated with loaded start-up in PMSM, the second case was designed where the motor starts under a load of 5 N·m at 1000 r/min, and the simulation results are shown in Fig. 5.

As illustrated in Fig. 5, the improved STSMC exhibits an overshoot of 8.221 r/min in rotational speed, stabilizing at the set value only after 0.0115s. The detailed value of performance indexes are given in Table 5. In Table 5, the overshoot of STSMC is 0.82 %, a decrease of 97.7 % compared to PI control and a reduction of 79.6 % compared to ST. In terms of response speed, the settling time of STSMC is 0.01s, which is 75.9 % faster than PI control and 17.3 % faster than ST. In terms of steady-state performance, the steady-state error of STSMC is 0.029 r/min, which is 69.8 % smaller than PI control and 47.3 % smaller than ST. These results demonstrate that

Table 3
Performance index during sudden load increase.

Control method	Peak RPM/ (r/min)	RPM overshoot/(%)	Settling time/(s)	Steady-state error/(r/min)	Torque overshoot/($\text{N} \cdot \text{m}$)
PI	927.292	7.271	0.031	0.317	0.034
SMC	976.256	2.374	0.016	0.05	0.004
ST	982.666	1.733	0.012	0.043	0.002
STSMC	982.823	1.718	0.008	0.027	0.001

Table 4
Performance index during sudden load decrease.

Control method	Peak RPM/ (r/min)	RPM overshoot/(%)	Settling time/(s)	Steady-state error/(r/min)	Torque overshoot/(N • m)
PI	1072.604	7.26	0.032	0.315	0.038
SMC	1024.281	2.428	0.015	0.052	0.004
ST	1017.837	1.784	0.012	0.043	0.002
STSMC	1016.93	1.693	0.008	0.018	0.001

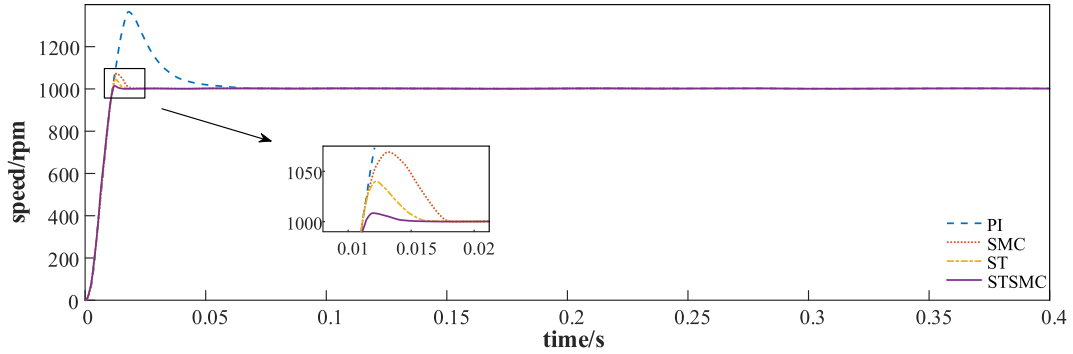


Fig. 5. Simulation results for case 2.

Table 5
Performance index during the start-up of case 2.

Control method	Peak RPM/ (r/min)	RPM overshoot/(%)	Settling time/(s)	Steady-state error/(r/min)	Torque overshoot/(N • m)
PI	1360.102	36.01	0.0477	0.096	8.168
SMC	1068.14	6.814	0.0164	0.064	6.345
ST	1040.229	4.03	0.0139	0.055	4.698
STSMC	1008.221	0.822	0.0115	0.029	1.441

during a loaded start-up, STSMC can reach steady state more quickly and with less oscillation.

4.3. Case 3: variable speed with no-load condition

To address the frequent speed changes of PMSM during operation, the third case was designed such that the motor starts at no load at 500 r/min, and at 0.2s, the reference speed abruptly changes to 1000 r/min. This case is used to verify that the proposed STSMC has better dynamic performance. The simulation results are shown in Fig. 6.

As shown in Fig. 6, the proposed STSMC exhibits an overshoot of 22.636 r/min as the speed increases to 1000 r/min. By $t = 0.2078s$, the motor speed has settled at the designated value of 1000 r/min. The detailed value of performance indexes are given in Table 6. In Table 6, the STSMC outperforms both traditional PI control and ST, with an overshoot of 2.264 %, which is an 85.1 % and 19.2 % reduction respectively. Furthermore, in terms of responsiveness, STSMC achieves a settling time of 0.0078s, which is 72.6 % faster than PI control and 11.4 % faster than SMC. During the variable speed experiment, ST exhibited a smaller overshoot compared to SMC, and SMC showed a shorter settling time than ST. However, STSMC was optimal in both overshoot and settling time, combining the advantages of both. Therefore, STSMC demonstrates superior variable speed performance compared to other methods.

4.4. Case 4: load with time-varying disturbance

In this case, PMSM was operated at a high rotational speed of 40000r/min. To simulate the time-varying disturbances that are typically encountered in such high-speed domains, a triangular wave disturbance of 2.5 N • m amplitude and 10 Hz frequency was introduced into the load. This was done to validate the robustness of STSMC to time-varying disturbances. The simulation results are shown in Fig. 7.

As indicated in Fig. 7, fluctuations in rotational speed are observed in the other three control methods. Specifically, PI control exhibits speed oscillations between 38275.8 r/min and 41624 r/min, with a maximum deviation of approximately 4.31 % from the target speed of 40000 r/min. SMC control experiences variations ranging from 39564.2 r/min to 40374.8 r/min, showing a maximum deviation of about 1.09 %. Meanwhile, ST control undergoes fluctuations within the 39311.3 r/min to 40550 r/min interval, resulting in a maximum deviation of approximately 1.72 % from the target speed. Conversely, the rotational speed of the improved STSMC remains stable, with no discernible fluctuations. The simulation results demonstrate that, even under the influence of a time-varying

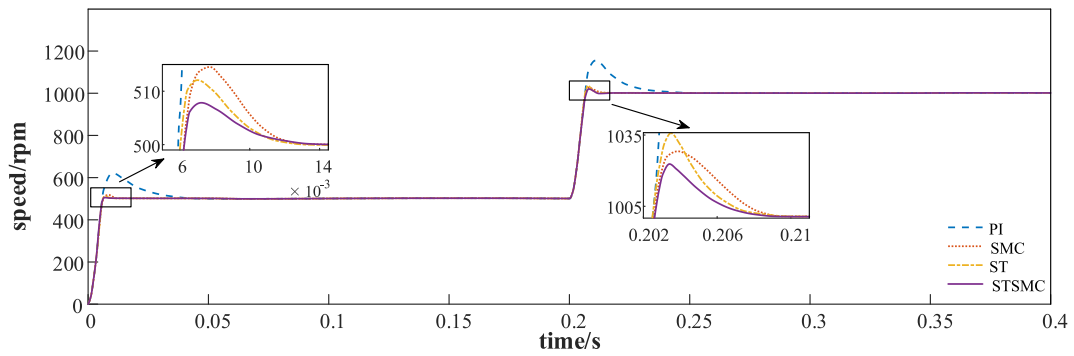


Fig. 6. Simulation results for case 3.

Table 6
Performance index during sudden speed increase.

Control method	Peak RPM/ (r/min)	RPM overshoot/(%)	Settling time/(s)	Steady-state error/(r/min)	Torque overshoot/(N • m)
PI	1152.016	15.202	0.0285	0.203	4.038
SMC	1035.692	3.569	0.0088	0.063	2.561
ST	1028.016	2.802	0.0095	0.078	4.986
STSMC	1022.636	2.264	0.0078	0.045	2.365

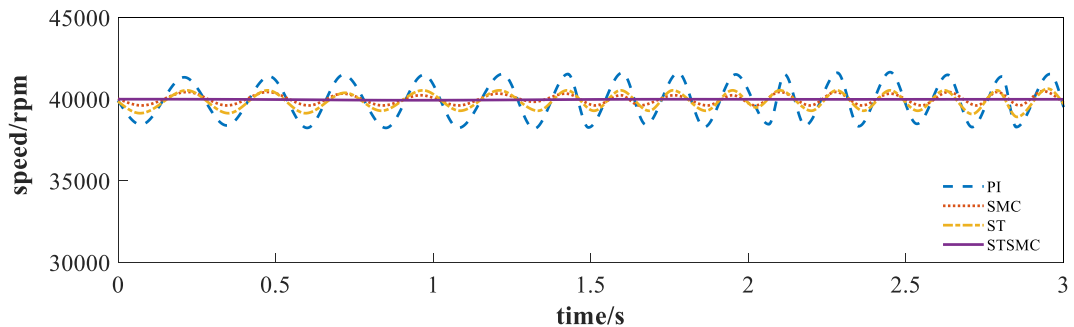


Fig. 7. Simulation results for case 4.

load torque, the improved STSMC exhibits better disturbance rejection capabilities compared to other three methods.

In conventional SMC, the reach time of the equivalent phase is affected by both the initial error and the switching coefficient, whereas the sliding surface coefficient influences the sliding phase's convergence speed. Although the SMC exhibits an exponential convergence process during the sliding phase, it requires infinite time to achieve full convergence - a conclusion derived from the sliding surface differential equation. Unlike the conventional SMC, the proposed STSMC incorporates a non-linear approach law, which modifies the way error phase trajectories converge towards the sliding surface.

Both the classical ST and improved STSMC centrally rely on the concept of relative level, employing the sliding surface as a control variable to accelerate convergence speed. However, the absence of linear term in the ST causes a slowdown in the convergence speed when approaching the reference point.

According to the above analysis of the simulation results, it can be found that the proposed STSMC exhibits superior robustness and expedited convergence, contributing to improved system performance. It proves particularly effective in addressing operational challenges, including sudden load changes, heavy-load startup, and frequent speed variations, thereby ensuring superior adaptability under diverse external conditions.

5. Conclusion

This paper proposed an improved STSMC strategy tailored to the complex operating conditions and pronounced internal environmental disturbances of hydrogen fuel cell centrifugal compressors, particularly for the associated PMSM. It specifically utilizes a combined GWO and BAS algorithm to optimize the parameter selection of the proposed STSMC. As verified in case studies, the proposed strategy demonstrates superior performance in handling disturbances, achieving rapid stabilization, and maintaining precise control compared to the existing algorithms. In variable load and high-speed domain scenarios, STSMC exhibited improved robustness

and adaptability, particularly in reducing overshoot, accelerating settling times, and minimizing steady-state errors under variable loads and during loaded start-ups. Moreover, STSMC effectively mitigated time-varying disturbances in high-speed operations, showcasing its superior disturbance rejection capabilities, crucial for complex operational environments and fluctuating operational demands for hydrogen fuel cell centrifugal compressor. Future work includes improvements to the controller of the current loop to further enhance the performance of the motor, effectively limit the armature current under sudden conditions and enhance the safety of the system.

Data availability statement

Data will be made available on request.

CRediT authorship contribution statement

Li Dong: Supervision, Project administration, Investigation, Funding acquisition, Formal analysis, Data curation, Conceptualization. **Pei Jiang:** Writing - review & editing, Writing - original draft, Visualization, Validation, Software, Resources, Methodology.

Declaration of competing interest

The authors declare that they have no known competing financial interests or personal relationships that could have appeared to influence the work reported in this paper.

References

- [1] Yong, Ying Jia, et al., A review on the state-of-the-art technologies of electric vehicle, its impacts and prospects, *Renew. Sustain. Energy Rev.* 49 (2015) 365–385.
- [2] Jiuyu Du, Minggao Ouyang, Jingfu Chen, Prospects for Chinese electric vehicle technologies in 2016–2020: ambition and rationality, *Energy* 120 (2017) 584–596.
- [3] Alexandre Beaudet, et al., Key challenges and opportunities for recycling electric vehicle battery materials, *Sustainability* 12 (14) (2020) 5837.
- [4] Simon T. Thompson, et al., Direct hydrogen fuel cell electric vehicle cost analysis: system and high-volume manufacturing description, validation, and outlook, *J. Power Sources* 399 (2018) 304–313.
- [5] Yuehua Li, et al., Analysis of air compression, progress of compressor and control for optimal energy efficiency in proton exchange membrane fuel cell, *Renew. Sustain. Energy Rev.* 133 (2020) 110304.
- [6] Hanwoong Ahn, et al., A review of state-of-the-art techniques for PMSM parameter identification, *J. Electr. Eng. Technol.* 15 (2020) 1177–1187.
- [7] Mohd Zaihidee, Fardila, Saad Mekhilef, Marizan Mubin, Robust speed control of PMSM using sliding mode control (SMC)—a review, *Energies* 12 (9) (2019) 1669.
- [8] Kifayat Ullah, Jaroslaw Guzinski, Adeel Feroz Mirza, Critical review on robust speed control techniques for permanent magnet synchronous motor (PMSM) speed regulation, *Energies* 15 (3) (2022) 1235.
- [9] Yongchang Zhang, Jialin Jin, Lanlan Huang, Model-free predictive current control of PMSM drives based on extended state observer using ultralocal model, *IEEE Trans. Ind. Electron.* 68 (2) (2020) 993–1003.
- [10] Marcel Nicola, Claudiu-Ionel Nicola, Tuning of pi speed controller for pmsm control system using computational intelligence, in: 2021 21st International Symposium on Power Electronics (Ee), IEEE, 2021.
- [11] Changhong Jiang, et al., Nonsingular terminal sliding mode control of PMSM based on improved exponential reaching law, *Electronics* 10 (15) (2021) 1776.
- [12] Dongliang Ke, et al., Predictive current control for PMSM systems using extended sliding mode observer with Hurwitz-based power reaching law, *IEEE Trans. Power Electron.* 36 (6) (2020) 7223–7232.
- [13] Xin Guo, et al., An improved integral sliding mode control for PMSM drives based on new variable rate reaching law with adaptive reduced-order PI observer, *IEEE Trans. Transport. Electrification* (2023).
- [14] Yuxiang Ma, et al., A novel discrete compound integral terminal sliding mode control with disturbance compensation for PMSM speed system, *IEEE ASME Trans. Mechatron.* 27 (1) (2021) 549–560.
- [15] Zhiqiang Liu, Wenkai Chen, Research on an improved sliding mode observer for speed estimation in permanent magnet synchronous motor, *Processes* 10 (6) (2022) 1182.
- [16] Bo Xu, Lei Zhang, Wei Ji, Improved non-singular fast terminal sliding mode control with disturbance observer for PMSM drives, *IEEE Trans. Transport. Electrification* 7 (4) (2021) 2753–2762.
- [17] Fardila M. Zaihidee, Saad Mekhilef, Marizan Mubin, Application of fractional order sliding mode control for speed control of permanent magnet synchronous motor, *IEEE Access* 7 (2019) 101765–101774.
- [18] Shihong Ding, Qiankang Hou, Hai Wang, Disturbance-observer-based second-order sliding mode controller for speed control of PMSM drives, *IEEE Trans. Energy Convers.* 38 (1) (2022) 100–110.
- [19] Qiankang Hou, Shihong Ding, Xinghuo Yu, Composite super-twisting sliding mode control design for PMSM speed regulation problem based on a novel disturbance observer, *IEEE Trans. Energy Convers.* 36 (4) (2020) 2591–2599.
- [20] Yong-Chao Liu, et al., Disturbance-observer-based complementary sliding-mode speed control for PMSM drives: a super-twisting sliding-mode observer-based approach, *IEEE J. Emerg. Select. Top. Power Electron.* 9 (5) (2020) 5416–5428.